A Simple Model of a Convectively Coupled Walker Circulation Using the Weak Temperature Gradient Approximation

CHRISTOPHER S. BRETHERTON

Department of Atmospheric Sciences, University of Washington, Seattle, Washington

ADAM H. SOBEL

Department of Applied Physics and Applied Mathematics, and Department of Earth and Environmental Sciences, Columbia University, New York, New York

(Manuscript received 9 November 2001, in final form 18 April 2002)

ABSTRACT

An idealized model of a Walker circulation based on the weak temperature gradient (WTG) approximation and a single baroclinic vertical mode for all fields is analyzed. The circulation is forced by a sinusoidal variation of sea surface temperature (SST). A simple feedback of deep convective cloud radiative forcing on tropospheric radiative cooling is included, and a moist convective adjustment is used to interactively specify the location and intensity of deep convection. A goal is to understand how the fraction of the domain undergoing deep convection depends on the SST difference across the domain.

The WTG approximation greatly simplifies the calculation of the circulation. For small SST differences, convection occurs everywhere and a fully analytic solution is possible; for larger SST differences, a simple nonlinear algorithm is used to determine the edge of the convective region and the tropospheric temperature. The solution is invariant to changes of domain size. The divergent circulation is independent of the Coriolis parameter as long as the domain is sufficiently narrow so WTG remains accurate.

The convective region narrows and intensifies considerably when cloud–radiation feedbacks are considered. As the SST difference increases, the convective region shrinks and the troposphere warms; simple approximate formulas for these trends in terms of the control parameters are derived. For large SST differences, the convection over the warmest water becomes susceptible to a radiative–convective instability and there is no steady-state solution.

1. Introduction

Simple ''two-box'' models of tropical climate feedbacks are based on a partitioning of the Tropics into moist, precipitating and dry, nonprecipitating regions (e.g., Pierrehumbert 1995; Miller 1997; Clement and Seager 1999; Larson et al. 1999). The areal fractions of each type of region are usually specified, and assumed not to vary as the climate forcing (e.g., greenhouse gases, aerosols, or insolation) changes. Since the precipitating and nonprecipitating regions have distinctly different mean thermodynamic and cloudiness profiles, area feedbacks could have a large impact on the sensitivity of tropical climate to forcing.

General circulation models (GCMs), our most sophisticated tool for looking at tropical climate variability, do internally predict convective area fraction. However, GCM-based sensitivity studies can be difficult to analyze and interpret. Intermediate-complexity tropical models in which the vertical thermodynamic structure of the troposphere is highly simplified, such as Neelin and Zeng's (2000, hereafter NZ00) quasiequilibrium tropical circulation model (QTCM) or the 2.5-layer model of Wang and Li (1993), are simpler to understand and can still produce a surprisingly realistic tropical climatology.

A further useful simplification suggested by scale analysis is the weak temperature gradient (WTG) approximation (Sobel and Bretherton 2000; Sobel et al. 2001), in which, to leading order, the tropical troposphere can be assumed to have horizontally uniform temperature, so that adiabatic cooling associated with vertical motion balances diabatic heating in all tropospheric air columns. This assumption is frequently made in two-box models, and has also been derived in some idealized models of the Hadley circulation (Fang and Tung 1996; Polvani and Sobel 2002). In this paper, we apply the WTG to a simplified version of an intermediate-level model (the QTCM) for an idealized Walker circulation in a nonrotating atmosphere driven by hor-

Corresponding author address: Dr. Christopher S. Bretherton, Department of Atmospheric Sciences, University of Washington, Box 351640, Seattle, WA 98195-1640.
E-mail: breth@atmos.washington.edu

izontally nonuniform SST, with and without deep cumulus cloud–radiation feedback. We compare our results with a cloud-resolving model (CRM) simulation of Grabowski et al. (2000, hereafter G00). Our main goals are (i) to show how the fractional area of precipitating convection is determined by the spatial distribution of SST, (ii) to understand the strong sensitivity of the precipitating area to cloud–radiation feedbacks, and (iii) to show the mathematical utility of the WTG for this problem.

Our approach has some similarities to an idealized Walker circulation model recently proposed by Kelly and Randall (2001). Although that model is formally a two-box model, it is similar to our model in that it incorporates a two-dimensional representation of the circulation in the descending branch, and it uses energy and water balance to determine a fractional area of deep convection. Unlike our model, their model includes an explicit representation of the cold-pool boundary layer physics. It also included a more elaborate treatment of radiative cooling. Our model is arguable easier to interpret and leads to different insights on the central parameters that control the circulation.

Our model is similar to that employed by Sobel et al. (2002, hereafter SHB), and described in their section 3. The main differences are that we treat the water budget consistently and that we include deep convective cloud feedbacks, both of which have major impacts on the precipitating area fraction.

2. Model equations

We look for a steady-state Walker circulation driven by specified SST variations in a slightly simplified version of the QTCM. Time integrations of the full QTCM forced as described below do reach reasonable steady states. However, a more complex model would produce only a statistically steady response, and one in which propagating disturbances such as a Madden–Julian Oscillation (MJO) might play a major role in the climatology.

We follow the notation of NZ00 where feasible. Temperature and specific humidity are expressed in energy units incorporating the heat capacity of air and latent heat of vaporization of water, respectively. Surface sensible and latent heat fluxes, tropospheric radiative flux divergence, and precipitation are expressed in energy flux units of W m^{-2}.

We consider a closed two-dimensional domain with walls at $x = 0, A$. Convection and circulation are forced by a specified surface temperature distribution $T_s(x)$ (again, expressed in energy units). For comparison with G00, we choose a sinusoidal structure with a maximum at $x = 0$ and a minimum at $x = A$:

$$T_s(x) = T_{s0} + T_{s1}(x),$$
$$T_{s1}(x) = c_p \Delta\mathrm{SST} \cos(\pi x/A). \quad (1)$$

We have retained more familiar temperature units for our primary control parameter ΔSST to make the figures easier to grasp. The methodology would apply just as well to any other monotonically decreasing SST profile.

The QTCM includes a barotropic and a baroclinic mode, but in two-dimensional geometry, the dynamics are purely baroclinic (except for a possible transverse barotropic y-velocity component that can be excited in the presence of Coriolis forcing combined with friction or nonlinearity). Hence, the temperature, specific humidity, x-velocity, and vertical p-velocity fields have fixed vertical structures:

$$\hat{T}(x, p) = T_{\mathrm{ref}}(p) + a(p)T(x), \quad (2)$$
$$\hat{q}(x, p) = q_{\mathrm{ref}}(p) + b(p)q(x), \quad (3)$$
$$\hat{u}(x, p) = V(p)u(x), \quad (4)$$
$$\hat{\omega}(x, p) = \Omega(p)\omega(x). \quad (5)$$

Here T_{ref} and q_{ref} are reference profiles and the nondimensional vertical structure functions a, b, V, Ω, shown in Figs. 1a,b are as in Zeng et al. (2000, with an additional subscript ''1'' and an extra factor of the inverse of the tropospheric pressure depth Δp_T in the definition of Ω_1). The basis functions are tailored to capture dominant modes of spatial variability in the Tropics. The temperature basis function represents the temperature perturbation between moist adiabats, reflecting the influence of moist convection. The moisture basis function is a compromise between the vertical moisture perturbations associated with moist convection and those associated with radiatively driven subsidence. The vertical structure function $V(p)$ is defined so that the direction of u is that of the upper-tropospheric x-wind component. The lower-tropospheric wind, which is predominantly responsible for advecting moisture, has the opposite sign. The vertical structure function $\Omega(p)$ is everywhere negative, so $\omega > 0$ corresponds to *upward* motion. The horizontal structure of the upper-tropospheric mass divergence and the vertical motion are given by

$$\omega/\Delta p_T = du/dx. \quad (6)$$

The QTCM equation for column-integrated moisture balance is

$$-\omega M_q/g = -P + E - (D_q \Delta p_T/g)u\, dq/dx. \quad (7)$$

Here M_q is the gross moisture stratification, a positive, horizontally varying quantity with units of J kg^{-1} proportional to the column-integrated moisture convergence per unit of upper-tropospheric mass divergence. The terms P and E are the precipitation and the surface evaporation (latent heat flux). The final term is the tropospheric column-integrated horizontal moisture advection defined as in NZ00's Eq. (5.12). The nondimensional coefficient D_q is defined as $D_q = \langle bV \rangle$, with angle brackets denoting a vertical average over the troposphere. All terms in this equation are retained in our model.

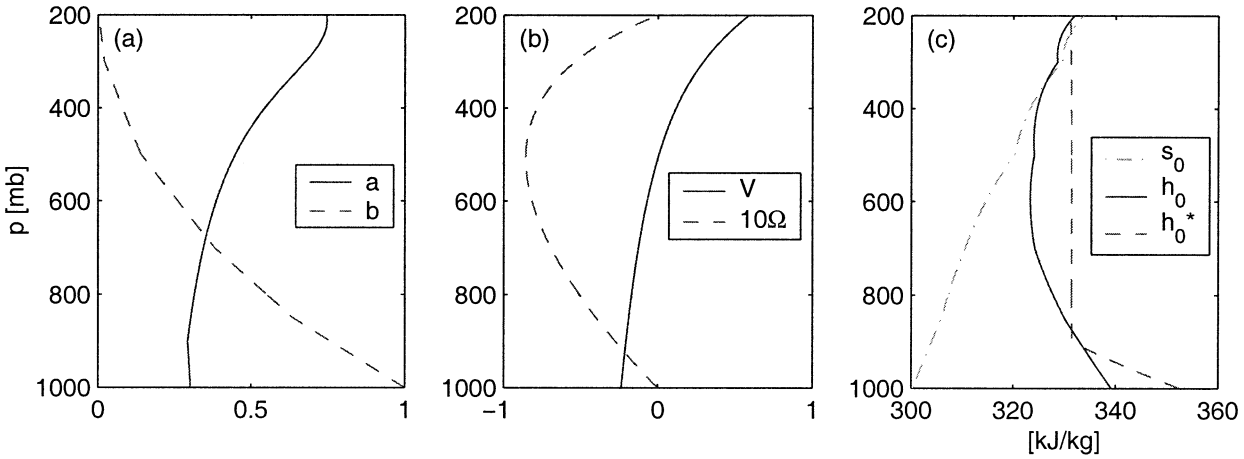

FIG. 1. QTCM basis functions for (a) temperature and humidity, (b) horizontal and vertical pressure velocity, and (c) reference radiative–convective equilibrium profiles for our model over an SST of 26°C. Plotted are dry static energy s_0, moist static energy h_0, and saturated moist static energy h_0^*.

The QTCM equation for column-integrated sensible heat balance is

$$\omega M_S/g = P - R + H - (D_T \Delta p_T/g)u\ dT/dx. \quad (8)$$

Here M_S is the gross dry stratification, which measures the column-integrated static energy divergence per unit of the upper-tropospheric mass divergence. Also, R is the radiative flux divergence across the troposphere, H is the sensible heat flux, and the final term is the column-integrated horizontal advection of dry static energy S, with the nondimensional coefficient $D_T = \langle aV \rangle$ defined as in NZ00's Eq. (5.11).

Here M_S and M_q are linear functions of T and q, respectively,

$$M_S = M_{Sr} + M_{Sp}T,$$

$$M_q = M_{qr} + M_{qp}q,$$

with M_{Sr}, M_{Sp}, M_{qr}, M_{qp} constants (see NZ00, sections 4c and 4d for derivation). It is straightforward to show that $M_{Sp} = D_T$ and $M_{qp} = -D_q$.

Adding (7) and (8), we obtain the moist static energy equation,

$$\frac{\omega M}{g} = E + H - R - \left(\frac{\Delta p_T}{g}\right)u\left(D_q\frac{dq}{dx} + D_T\frac{dT}{dx}\right), \quad (9)$$

where $M = M_S - M_q$ is the gross moist stability.

a. WTG approximation

We apply the WTG approximation that the tropospheric temperature is essentially uniform. This implies that T, though unknown, is independent of x. Hence, there is no horizontal advection of static energy, and the gross dry stability M_S is also x independent.

Conceptually, the WTG approximation dramatically simplifies our problem. In the QTCM, the heat equation in each atmospheric column is a prognostic equation for the tropospheric temperature in that column. Even in the steady state, this equation includes a nonlinear horizontal temperature advection term. The horizontal variations in temperature, though small, must be explicitly determined as part of the overall solution. This prevents a closed-form solution to the steady-state equations. In WTG, the corresponding heat equation reduces to a balance between horizontal energy divergence [proportional to $\omega(x)$] and energy convergence into the atmospheric column from surface turbulent fluxes and net radiative flux convergence. If simple forms are chosen for these fluxes, WTG yields a comparably simple expression for the spatial structure of the divergent flow in terms of a couple of easily understood parameters, clarifying the essential structure of the Walker circulation problem.

To close the model, we will now couple the moisture and temperature profiles within regions of deep convection, and specify forms for the turbulent and net radiative fluxes into the column. Our approach is to strive for mathematical simplicity without sacrificing the central feedbacks between deep convection, cloud, and radiation processes, and the large-scale circulation in a Walker circulation forced by known SST variations.

b. SQE assumption

For our convective parameterization, we assume "strict quasi-equilibrium" (SQE; e.g., Emanuel et al. 1994) in regions where deep convection occurs. The QTCM's Betts–Miller-like convective adjustment parameterization reduces to this limit as the convective adjustment time becomes small. In the QTCM notation, $q - T$ is the convective available potential energy (NZ00) so SQE implies that in regions of convective heating on precipitation,

$$q = T, \quad \text{where} \quad P > 0. \quad (10)$$

Since T is horizontally uniform, so is q within the convective region. The horizontal advection of moisture vanishes, and the gross moist stability M is also uniform across the convective region. The moist static energy balance (9) simplifies to

$$\omega M/g = E + H - R \tag{11}$$

in convective regions. Nonconvective regions must have $q < T$.

c. Surface fluxes

We parameterize the latent heat flux

$$E = c_q[q^*(p_s, T_s) - q_s], \tag{12}$$

where $q^*(p_s, T_s)$ is saturation-specific humidity at the sea surface pressure and temperature; q_s is the actual surface-specific humidity, related to q by (3); and c_q is a bulk exchange coefficient independent of wind speed. This assumption greatly simplifies our mathematical analysis, but is not entirely realistic and may prevent important feedbacks. In reality, c_q should depend on the model-predicted mean wind (e.g., Emanuel 1987; Neelin et al. 1987), the variability of the wind on synoptic timescales not addressed by this model, and mesoscale gustiness associated with the convection itself (Miller et al. 1992), which could provide a positive feedback between convection and evaporation. Hints of such a feedback are visible in G00's plot of surface fluxes from their CRM simulation.

We linearize the Clausius–Clapeyron equation about a reference SST T_{s0}:

$$q^*[p_s, T_s(x)] = q^*_{s0} + \gamma_s T_{s1}(x), \tag{13}$$

where $\gamma_s = (\partial q^*/\partial T_s)_0$, and subscript "0" indicates evaluation at the reference sea surface pressure and temperature.

For simplicity and consistency with SHB, we neglect the surface sensible heat flux,

$$H \approx 0, \tag{14}$$

since it is typically only 10% of the latent heat flux. A bulk formula for H analogous to (12) can be added to the analysis with minor additional complication.

d. Radiative heating

We parameterize the column-integrated clear-air radiative flux divergence by a Newtonian relaxation:

$$R^{\text{clr}} = \frac{\Delta p_T}{g}\frac{T - T_e}{\tau_R}, \qquad = R^{\text{clr}}_{\text{ref}} + c_R T. \tag{15}$$

Here, τ_R is a radiative timescale, T_e is a radiative equilibrium value of T (in energy units), $c_R = \Delta p_T/(g\tau_R)$ and $R^{\text{clr}}_{\text{ref}} = -c_R T_e$. We use $\tau_R = 25$ days, as in SHB. However, their radiative equilibrium temperature was chosen to fit tropical-mean cooling rates including both clear and cloudy regions. A colder T_e is needed to realistically specify clear-sky cooling. We chose $T_e = -51.2$ kJ kg^{-1} to obtain a tropospheric radiative flux divergence of 125 W m^{-2} in a radiative–convective equilibrium simulation (see section 3). We specified this value to match the specified troposphere-averaged radiative cooling rate of 1.5 K day^{-1} in the CRM simulations of G00. One might think that the clear-air column cooling would depend strongly on the column moisture. We did an analysis of the monthly mean clear-air flux divergence versus water vapor path over all tropical ocean columns (20°S–20°N) in a climatological run of the National Center for Atmospheric Research (NCAR) Community Climate Model, version 3.6. This showed only a weak systematic variation of 10–20 W m^{-2} between typical simulated moister and drier columns. Thus, we have not included a feedback of column moisture on clear-air cooling in our model. We have also neglected the impact of SST on the radiative equilibrium temperature of the troposphere, which is of comparable importance to surface sensible heat fluxes (Su and Neelin 2002).

We do allow for atmospheric cloud radiative forcing from deep convective cloud systems. Kiehl (1994) showed that top-of-atmosphere (TOA) short- and longwave cloud radiative forcing both increase linearly with the coverage of highly reflective clouds over the west Pacific warm pool. Here, we are interested in just the atmospheric cloud forcing, since we are specifying SST. Broadly speaking, the TOA shortwave cloud forcing is mainly felt as cooling of the ocean, and the TOA longwave cloud forcing is mainly felt as warming of the atmosphere. Since precipitation is highly correlated with highly reflective clouds, we assume that the atmospheric cloud radiative flux divergence is reduced in proportion to the precipitation:

$$R = R^{\text{clr}} - rP. \tag{16}$$

Convective clouds also have two counteracting cooling effects on the troposphere. First, they slightly reduce atmospheric shortwave absorption by reflecting sunlight before it can be absorbed by lower-tropospheric water vapor and clouds. Second, they slightly increase surface downwelling longwave radiation. These effects reduce the cloud–radiative feedback r, but they do not qualitatively affect its character.

To determine r, we use a Tropical Ocean Global Atmosphere Coupled Ocean–Atmosphere Reponse Experiment (TOGA COARE) radiation dataset for November 1992–February 1993 (Burks 1998). It is based on buoy measurements of surface radiation, and broadband radiances inferred from narrowband geostationary satellite imagery, and was assembled by P. Minnis and W. Rossow of the National Aeronautic and Space Administration (NASA). We compare this with precipitation inferred from moisture budgets over the TOGA COARE Intensive Flux Array (IFA; Lin and Johnson 1996). All

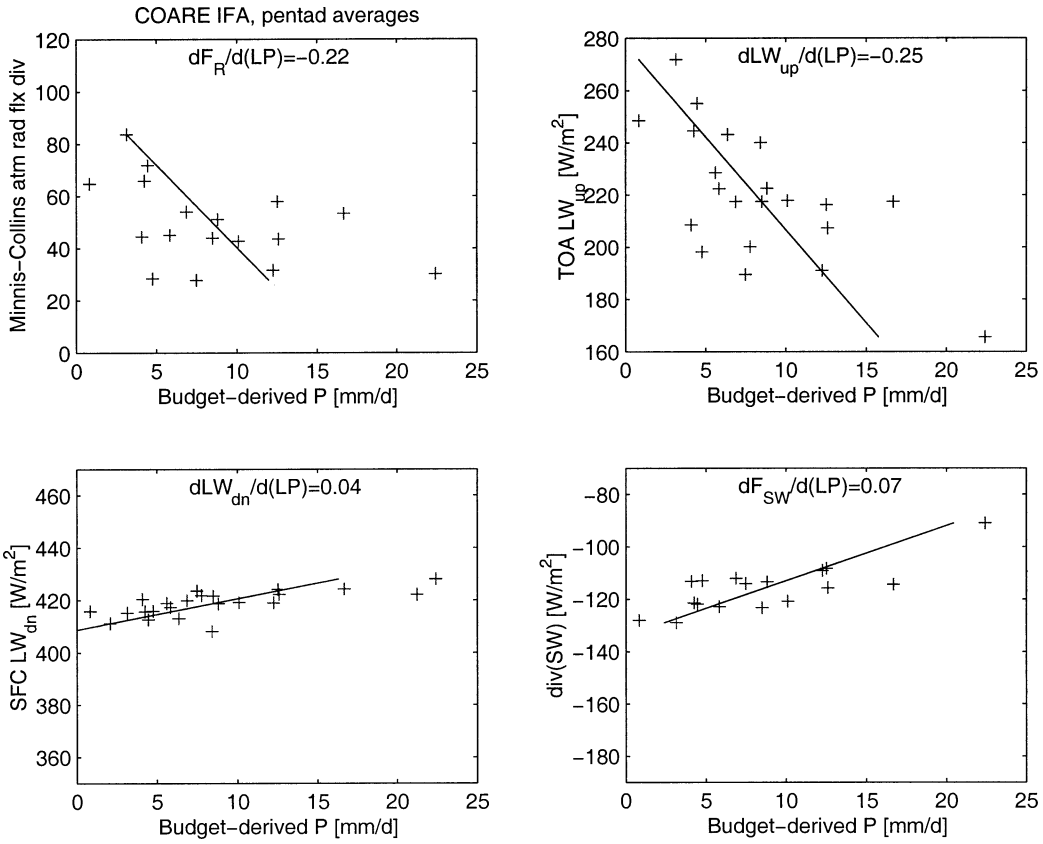

FIG. 2. Scatterplots of net atmospheric radiative heating, TOA and surface longwave radiative fluxes, and tropospheric shortwave absorption vs IFA-mean precipitation P for all pentads in which data are available during TOGA COARE (1 Nov 1992–28 Feb 1993). In each plot, the line is a least squares fit of P on the other plotted variable, and the line slope is given in the top center of each panel.

of these quantities are subject to substantial uncertainty and possible biases that we acknowledge but will not further discuss. We use 5-day-averaged values to smooth over individual convective systems and reduce the impact of random sampling errors. In Fig. 2, we show scatterplots of atmospheric column-integrated radiative flux divergence versus precipitation and its partitioning between the three main sources of variability—the TOA and surface longwave radiative fluxes and the shortwave absorption. Since the budget-derived IFA-mean precipitation is arguably the most uncertain quantity in this analysis, the regression lines use precipitation as the dependent variable, hence the three latter regression line slopes do not add up exactly to the regressed slope of net radiation versus precipitation.

The implied r of 0.22 is quite uncertain, though a trend is clear in the data. As argued above, the main contributor to r is the reduction of outgoing longwave radiation in precipitating regions; the other two terms cancel 30%–40% of this effect.

We also made a scatterplot (not shown) of monthly mean Earth Radiation Budget Experiment (ERBE) TOA longwave cloud forcing (LWCF) on satellite-derived monthly precipitation (Xie and Arkin 1997) over all tropical ocean points (20°S–20°N) and months. These datasets are not independent, but do show a tight linear relation with $d\text{LWCF}/d(LP) \approx 0.2$. This is in fair agreement with the COARE data, though it would suggest a slightly smaller value of r on the order of 0.15.

With all this in mind, we follow Fuchs and Raymond (2002) and take $r = 0.2$, with possible uncertainties up to 50%.

e. Momentum balance

The WTG approximation and the assumption that the surface fluxes do not depend on wind speed allow us to solve for the divergent circulation without the use of the momentum equations. This has the remarkable consequence that the divergent circulation is independent of both the Coriolis parameter and the surface frictional stress. Small horizontal pressure variations hydrostatically associated with small horizontal temperature variations $T'(x)$ are required to drive this flow. In WTG, $T'(x)$ is diagnosed from the momentum equation and adjusts as necessary to support the WTG-implied divergent flow. WTG will be consistent so long as the

TABLE 1. Model parameter values.

Parameter	Symbol	Value
Basic parameters		
Tropospheric pressure depth	Δp_T	800 hPa
Domain-average SST	T_{s0}	300.35 kJ kg^{-1} (26°C)
Bulk constant for evaporation	c_q	0.009 kg m^{-2}s^{-1}
Clear-air radiative equilibrium temperature	T_e	−51.2 kJ kg^{-1}
Radiative relaxation time	τ_r	25 days
Cloud–radiative heating feedback	r	0.2
Parameters from QTCM v2.2		
$dT(p_s)/dT_1$	a_s	0.302
$dq(p_s)/dT_1$	b_s	1.0
Reference gross dry stability	M_{Sr}	3520 J kg^{-1}
Reference gross moisture stratification	M_{qr}	3017 J kg^{-1}
dM_S/dT	M_{Sp}	0.0435
dM_q/dT	M_{qp}	0.0507
Momentum advection coefficient	D_V	0.2154
Frictional damping rate	ϵ	(3.43 days)$^{-1}$
Derived parameters		
RCE clear-sky radiative flux divergence	$R_0^{\rm clr}$	150 W m^{-2}
$dR^{\rm clr}/dT_1$	c_R	0.0038 (W m^{-2})/(J kg^{-1})
RCE precipitation/evaporation rate	$P_0 = E_0$	125 W m^{-2}
RCE gross dry stability	M_{S0}	3017 J kg^{-1}
RCE gross moisture stratification	M_{q0}	2431 J kg^{-1}
RCE gross moist stability	M_0	586 J kg^{-1}
Approx $dT_1/d\Delta$SST	a_1	2.32
Approx convective area fraction parameter	a_2	10.8 m^2 s kg^{-1}

required temperature perturbations remain small compared to the SST variations.

Given the divergent circulation $[u(x), \omega(x)]$, the transverse (rotational) wind component $v(x)$ can be found from the QTCM y-momentum equation (note there are no pressure gradients in the y direction). If there is no ambient rotation, $v = 0$. Otherwise, both baroclinic and barotropic structures in v are excited. For simplicity, we present only no-rotation solutions in the paper.

The steady-state QTCM x-momentum equation with Coriolis parameter f, Rayleigh damping rate ϵ, and ratio of dry air gas constant to isobaric specific heat $\kappa = R_d/c_p$, is

$$D_V\left(\frac{udu}{dx} + \frac{0.5\omega u}{\Delta p_T}\right) - fv = \left(\frac{R_d}{c_p}\right)\frac{\partial T'}{\partial x} - \epsilon u. \quad (17)$$

This is NZ00's Eq. (5.1), with their (5.12) substituted for the nonlinear advection term, their ϵ_1 and D^V_{111} renamed as ϵ and D_V, and with their vertical advection coefficient in (5.12) written in terms of D_V using an integration by parts. The values of D_V and ϵ that we used, taken directly from version 2.2 of the QTCM, are given in Table 1. Here $T'(x)$ is the temperature perturbation from WTG that hydrostatically produces the baroclinic pressure gradients necessary to drive the circulation. Given the velocity field, (17) is a first-order differential equation that can be numerically integrated from $x = 0$ to the outer boundary to determine T'. The T' is determined only up to an additive constant; to make T' unique we require it to have a domain average of zero.

3. Radiative–convective equilibrium state

NZ00 used a characteristic disturbed tropical sounding $[T_{\rm ref}(p), q_{\rm ref}(p)]$ as their reference state. We instead adopt the radiative–convective equilibrium (RCE) of our model above the domain-averaged SST T_{s0} as our reference state $[T_0(p), q_0(p)]$. The RCE profiles differ from those used in NZ00 by multiples of $a(p)$ and $b(p)$ of a saturation moist static energy offset h_0^*, respectively,

$$T_0(p) = T_{\rm ref}(p) + a(p)h_0^*, \quad (18)$$

$$q_0(p) = q_{\rm ref}(p) + b(p)h_0^*. \quad (19)$$

This offset is calculated from steady-state energy and moisture balance:

$$P_0 = R_0 = E_0. \quad (20)$$

Substituting (16) into the first equality above,

$$R_0 = R^{\rm clr} - rP_0, \quad (21)$$

$$P_0 = R^{\rm clr}/(1 + r) = (R^{\rm clr}_{\rm ref} + c_R h_0^*)/(1 + r). \quad (22)$$

Next we substitute (12) for the evaporation. Denoting $b_s = b(p_s)$, we obtain

$$E_0 = c_q(q^*_{s0} - q_{\rm ref}(p_s) - b_s h_0^*). \quad (23)$$

We solve for h_0^* by equating this expression for E_0 with P_0, as given by (22).

For the basic parameters chosen in Table 1, we find $h_0^* = -11.5$ kJ kg^{-1}, yielding the RCE dry and moist static energy profiles shown in Fig. 1c. The surface relative humidity is 77%, and the air temperature is 0.6 K

colder than the SST. Given our choice of bulk transfer rate c_q, this would drive a sensible heat flux of less than 5 W m^{-2}; this is a posteriori justification for the neglect of surface sensible heat flux in our model. The RCE precipitation rate and gross stabilities are listed as derived parameters in Table 1, as they will be needed for the subsequent analysis.

4. Solution for small ΔSST

We now consider a slight cosine-shaped horizontal SST modulation with amplitude ΔSST, defined by (1) and denoted as $T_{s1}(x)$ in energy units. For thermodynamic variables with nonzero means, we denote deviations from RCE with a subscript 1, so that the temperature difference from the QTCM reference profile is $T = T_0 + T_1$, and similarly for humidity. This is analogous to the notation of NZ00, but with their reference profile replaced by our RCE profile. We anticipate upward motion and enhanced precipitation over the warmer water, and downward motion and reduced precipitation over the colder water. However, for sufficiently small T_{s1}, we expect some convection everywhere, as long as RCE is a stable equilibrium. Hence, $q_1 = T_1$ and both are horizontally uniform, as is M.

We can use the moist static energy budget (11) with our idealizations for the surface fluxes to deduce the vertical motion $\omega(x)$ throughout:

$$\omega M/g = E_1(x) - R_1(x), \tag{24}$$

$$E_1 = c_q[\gamma_s T_{s1}(x) - b_s T_1], \tag{25}$$

$$R_1 = -rP_1 + c_R T_1. \tag{26}$$

To find the cloud–radiation feedback term, we must simultaneously solve for the precipitation perturbation from RCE, $P_1(x)$, using the moisture budget (7):

$$P_1 = E_1 + \omega M_q/g. \tag{27}$$

Substituting this into (26), we can express $\omega(x)$ and precipitation in terms of known, x-varying, quantities and a single unknown T_1:

$$\omega_c(x) = g\frac{c_q\gamma_s(1 + r)T_{s1}(x) - [c_q b_s(1 + r) + c_R]T_1}{M - rM_q}, \tag{28}$$

$$P(x) = P_0 + E_1(1 + C) - c_R C T_1/(1 + r), \tag{29}$$

$$C(T_1) = \frac{M_q(1 + r)}{M - rM_q}. \tag{30}$$

The horizontal modulation of precipitation can be partitioned into a term due to enhancement of local evaporation over warmer SST, and a second term due to "convergence feedback" (Zebiak 1986; Sobel and Bretherton 2000), in which local surface evaporation into a convecting atmospheric column is reinforced by anomalous horizontal convergence of moisture. Specifically, to maintain column moist static energy balance in the face of increased surface latent heat fluxes, there must be a proportional net export of moist static energy, which occurs through low-level mass convergence and upper-level divergence, resulting in net convergence of moisture into the column. The nondimensional parameter $C(T_1)$ measures the convergence feedback. It is sensitive to both the cloud–radiation feedback r and the tropospheric temperature T_1. The convergence feedback parameter in RCE ($T_1 = 0$), using the parameters of Table 1, is $C_0 = 4.2$ without cloud–radiation feedback, but 29 with cloud–radiation feedback.

The convergence feedback can be expressed in the form

$$C = M_q/M_{\text{eff}}, \tag{31}$$

$$M_{\text{eff}}(T_1) = (M - rM_q)/(1 + r). \tag{32}$$

One can regard M_{eff} as an effective gross moist stability including radiative feedbacks. A similar parameter (but without the denominator $1 + r$) was introduced by Su and Neelin (2002). For our parameters, M_{eff} is 83 J kg^{-1} at RCE, only 17% as large as M. Because M_{eff} is the difference of two nearly canceling terms, it is highly sensitive to changes in r or the RCE humidity profile. The M_{eff} decreases linearly with T_1, passing through zero at $T_1^{\text{RCI}} = 5$ kJ kg^{-1}. Thus, the convergence feedback increases rapidly with tropospheric temperature, becoming infinite at T_1^{RCI}. The radiative–convective instability regime $M_{\text{eff}} < 0$ seems easily reachable in parts of the Tropics, where M may be smaller or cloud feedbacks slightly stronger. No steady-state solution with $T_1 > T_1^{\text{RCI}}$ is possible. In this regime a region of convection over uniform SST would spontaneously break down into patches of more and less intense convection. This feedback, discussed by Raymond (2000) in a model of the Hadley circulation, would ultimately be limited by saturation of the longwave radiative feedback as the thick anvil cirrus cloud cover reaches 100%.

If we average across the entire domain, the SST perturbation $T_{s1}(x)$ averages to zero. Mass conservation dictates that ω must also average to zero. The stabilities M and M_q are horizontally uniform since they depend only on T_1. Thus, (28) implies that when there is convection over the entire domain, $T_1 = q_1 = 0$: the tropospheric temperature and humidity are everywhere the same as in the radiative–convective equilibrium.

Figure 3 shows the horizontal variation of vertical motion and precipitation with and without the radiative feedback for ΔSST = 0.1 K and the parameters given in Table 1. There is a sixfold radiative enhancement of the vertical motion perturbations corresponding to the sixfold increase in the convergence feedback parameter C.

For SST variations exceeding the threshold,

$$\Delta\text{SST}^{\text{crit}} = \frac{P_0}{c_p c_q \gamma_s(1 + C_0)}, \tag{33}$$

the above solution breaks down by predicting negative precipitation over the coldest water. For our parameter

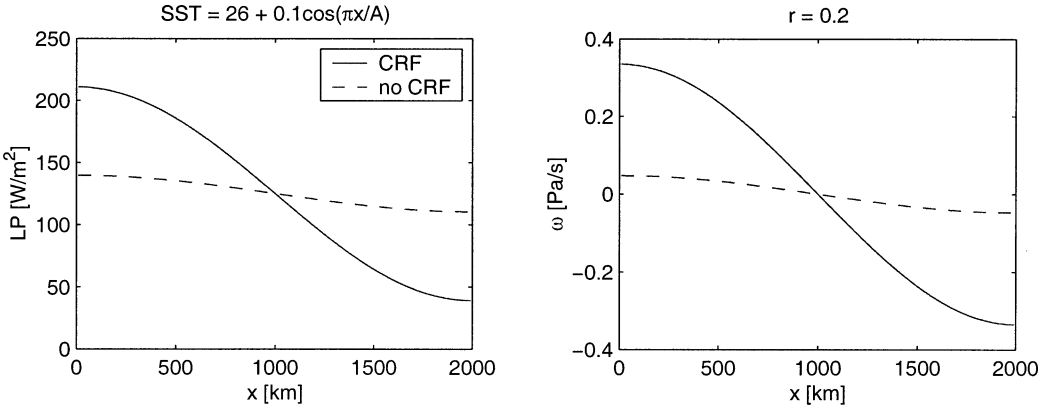

FIG. 3. (left) Modeled precipitation and (right) $\omega(x)$ for ΔSST = 0.1 K. Convection extends throughout the domain. Actual vertical p velocity is obtained by multiplying ω by the vertical structure function $\Omega(p)$ of Fig. 1b, which varies from 0 at the surface and tropopause to an extremum of -0.09 at 500 mb. The solid and dashed curves show steady-state solutions including and excluding CRF, respectively.

values, $\Delta\text{SST}^{\text{crit}} = 0.14$ K with cloud–radiation feedback and 0.86 K without this feedback. If the SST modulation exceeds this modest level, a nonconvecting region forms over the colder water, necessitating a more involved solution procedure described in the next section.

5. Solution for larger ΔSST

For $\Delta\text{SST} > \Delta\text{SST}^{\text{crit}}$, we seek a solution with convection, precipitation, and $q_1 = T_1$ for $x < A_c$, and no convection and $q_1 < T_1$ for $A_c < x < A$. The tropospheric temperature deviation T_1 from the reference state and the convective edge A_c are unknowns determined by requiring that the solution obey global moisture and heat balance (the latter is also equivalent to mass conservation in WTG).

We first derive heat and moisture conservation equations in the nonconvective region, denoted by the subscript nc. The sensible heat budget (8) is a balance between subsidence and clear-air radiative cooling, implying uniform subsidence:

$$\omega_{\text{nc}} = -gR^{\text{clr}}/M_S. \tag{34}$$

Mass continuity implies that the horizontal velocity increases linearly with distance away from the outer boundary at $x = A$:

$$u_{\text{nc}}(x) = -(A - x)\omega_{\text{nc}}/\Delta p_T. \tag{35}$$

The moisture balance equation (7) reduces to a balance between vertical and horizontal advection and evaporation:

$$-\omega_{\text{nc}}M_q(x) = gE(x) - D_q\Delta p_T u(x)\, dq_1/dx. \tag{36}$$

Substituting (34) for ω and (25) for E in this equation, and multiplying by g, we obtain a first-order ordinary differential equation for the humidity perturbation $q_1(x)$ away from RCE:

$$-c_1(A - x)dq_1/dx + c_0 q_1 = F_q(x), \tag{37}$$

where (recalling that $D_q = -M_{qp}$),

$$c_1 = -\omega_{\text{nc}}M_{qp},$$

$$c_0 = -\omega_{\text{nc}}M_{qp} + gc_q b_s$$

$$F_q(x) = g[E_0 + c_q\gamma_s T_{s1}(x)] + \omega_{\text{nc}}M_{q0}.$$

This differential equation is singular at the outer boundary where $u(A) = 0$. There is a unique solution that is finite at A. For this solution, (37) implies that $q_1(A) = F_q(A)/c_0$. For constant c_q, the differential equation can be integrated analytically, but we adopt a straightforward numerical integration approach that can be adapted for variable c_q. We discretize (37) and march q_1 inward from $x = A$. The integration is terminated where $q_1(x)$ first exceeds T_1, signalling the edge $x = A_c(T_1)$ of the convective region.

The trial solution is extended toward smaller x in the convective region using the moist static energy equation (28) to determine $\omega_c(x)$. Mass and heat balance are achieved for that T_1 for which

$$0 = \int_0^{A_c(T_1)} \omega_c(x)\, dx + [A - A_c(T_1)]\omega_{\text{nc}}. \tag{38}$$

We have always found a unique solution T_1, but we have not tried to prove that this will necessarily be the case.

This general solution method could be extended to the case where c_q depends on u by integrating $u(x)$ inward from the convective edge using mass continuity at the same time we determine $\omega_c(x)$. Other extensions, such as generalization to a more realistic parameterization that column-integrated humidity q_1 in the convective region depends not only on T_1 but also the local intensity of convection as measured for instance by P, could also be easily incorporated.

a. Results

The solid line in Fig. 4 shows a ''control'' solution with $\Delta\text{SST} = 2$ K and $r = 0.2$. This solution can be

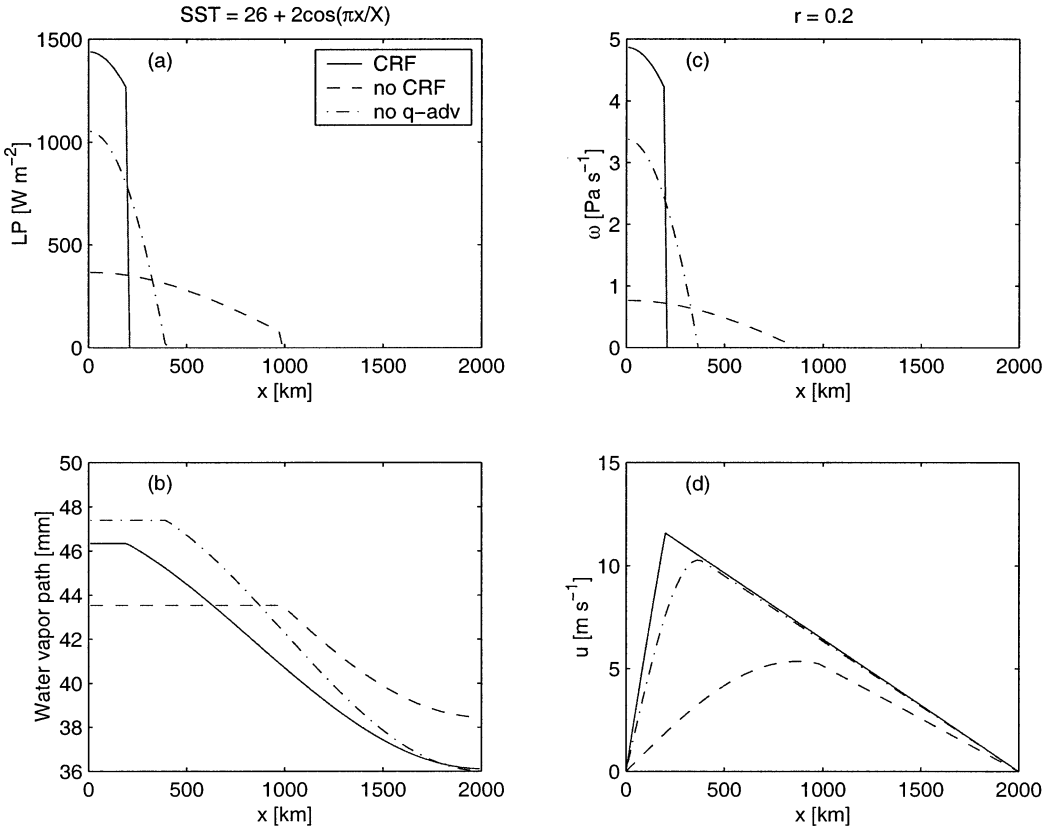

FIG. 4. (a) Precipitation, (b) water vapor path, (c) vertical motion, and (d) horizontal motion for ΔSST = 2 K. In the latter two panels, the full two-dimensional fields are obtained by multiplying by the vertical structure functions $\Omega(p)$ and $V(p)$ shown in Fig. 1b, respectively.

compared with G00's interactive radiation cloud-resolving model simulation. A narrow region of intense convection forms over the warmest SSTs. Its width, 200 km, is similar to that found in G00's simulation. The increased mean SST of the convective region is also reflected in a comparable tropospheric temperature increase from RCE (T_1 = 3.1 kJ kg^{-1}, corresponding to an air temperature increase of 1 K in the boundary layer and lower troposphere and 2 K in the upper troposphere). It is noteworthy that the precipitation and vertical motion are discontinuous at the edge of the convective region. The vertical and horizontal velocity variables must be multiplied by their nondimensional vertical structure functions (Fig. 1b) to obtain the true velocities. For horizontal velocities, this structure function varies from -0.25 at the bottom to 0.5 at the top. The maximum implied near-surface mean winds are only 3 m s^{-1}, and a realistic bulk surface transfer coefficient for moisture flux would also reflect comparable contributions to the total wind speed from synoptic variability and convective gustiness, so the assumption of constant c_q is not implausible for this case. The structure function for vertical motions is zero at the top and bottom and reaches a minimum of -0.09 at 500 mb, so in the core of the convective region the midtropospheric ω is roughly -0.5 Pa s^{-1} with intense precipitation of roughly 50 mm day^{-1}. This precipitation rate is higher than the observed monthly climatology for any part of the Tropics, but it is extremely sensitive to the assumed cloud–radiation feedback and the gross moist stability. If r were decreased 20% and the RCE gross moist stability were increased 20%, maximum precipitation rates within the convective region would decrease to more realistic levels. However, our goal here is to note the sensitivities of the solution rather than to strive for complete realism.

The dashed line in Fig. 4 shows a simulation with cloud radiative feedback removed (r = 0) and the reference clear-sky radiative flux divergence is reduced by 25 W m^{-2} to produce the same mean precipitation in a RCE simulation. As in G00, the convective region broadens substantially to a width of nearly 1000 km, and the precipitation in this region weakens. The broader convective region implies a broader SST range and lower SST threshold for convection, which is consistent with the cooler troposphere (T_1 reduced to only 0.9 kJ kg^{-1}).

The dot–dashed line in Fig. 4 shows a simulation like the control but with horizontal moisture advection neglected as in SHB by setting c_1 = 0 in (37). The con-

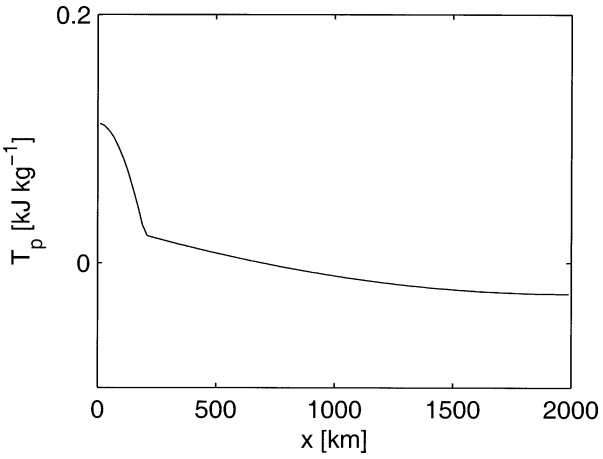

FIG. 5. Horizontal structure of the tropospheric temperature variation (in energy units) associated with the Walker circulation of Fig. 4, deduced using from WTG using the horizontal momentum equation. To obtain the two-dimensional temperature field, multiply by the vertical structure function $a(p)$ of Fig. 1a.

vective region is somewhat broadened and the precipitation and vertical motion are now continuous across the convective edge. However, the tropospheric temperature and the minimum water vapor path in the nonconvective region are quite similar to the control solution. The tropospheric temperature increase from RCE is 3.9 kJ kg^{-1}, 20% larger than the control solution. The water vapor path is also slightly larger than the control. The comparative insensitivity of these bulk properties of the Walker circulation to the moisture advection is due to the dominance of local evaporation over drying by horizontal advection in the dry region (i.e., $c_1 \ll c_0$). The evaporation ranges from 110 W m^{-2} at the outer wall to 155 W m^{-2} in the convective region. The column-integrated advective drying increases from 0 W m^{-2} at the outer wall of the domain to only about 20 W m^{-2} at the convective edge, and is 0 W m^{-2} within the convective region.

Clearly, some aspects of these simulations differ significantly from reality. In addition to the intensity of precipitation in the convective region, the model has a different distribution of surface evaporation than observed. Observed surface evaporation tends to be largest in trade cumulus regions rather than in the deep convective regions of the Tropics, owing to the higher mean wind speeds. The vertical moisture structure in the trades is also oversimplified in the model. However, we believe that this model still provides a useful guide for understanding the response of the Walker circulation to changes in its forcing.

b. Solving for horizontal pressure perturbations

Figure 5 shows the tropospheric temperature perturbation $T'(x)$ from WTG in a nonrotating atmosphere implied by the x-momentum equation (17) forced by the circulation in the control run. The maximum value is about 0.1 K, which is indeed much smaller than the SST range. Hence the WTG approximation should be accurate for this simulation. The warmest temperature perturbation (lowest surface air pressure) is over the warmest SST, as expected for a thermally direct circulation. The implied surface air pressure difference across the domain, $\Delta p_s = -\rho_s R_d[T'(A) - T'(0)]V(p_s)/c_p$, is about 0.1 hPa.

c. Scaling properties of WTG solutions

An interesting feature of our WTG solutions is their invariance to changes in domain size. If the domain size A were changed, the fractional area of convection would be unchanged. If plotted in the scaled horizontal coordinate x/A, so would the precipitation, vertical motion, and humidity fields. The horizontal moisture advection is similarly invariant, being the product of a horizontal velocity that scales with A, and a humidity gradient that scales with A^{-1}. The implied temperature perturbation T' from WTG scales as A^2, as does the horizontal temperature advection. If A becomes large enough (10 000 km for the example above), WTG starts to break down due to the large temperature perturbations $T'(x)$. In reality, WTG holds fairly well even on a global scale in the free troposphere (Sobel and Bretherton 2000). This is because little of the surface stress is actually communicated to the free troposphere (Carr and Bretherton 2001), reducing the pressure gradients required to drive the required divergent wind field. In the boundary layer, stronger turbulent Reynolds stress convergence (drag) is balanced by stronger pressure gradients produced by the Lindzen–Nigam (1987) mechanism—the boundary layer air temperature is strongly controlled by SST, hydrostatically driving substantial near-surface pressure gradients even though the free-tropospheric pressure gradients are small.

For the Hadley circulation, our WTG model with specified SSTs does not provide any obvious horizontal length scale. Coriolis forces do help produce horizontal gradients in $T'(x)$ that would render WTG inconsistent over a sufficiently broad meridionally oriented domain. At larger latitudes, the rotational wind implied by the WTG-predicted zonal wind also becomes very large, and in reality will have a strong impact on surface moisture and heat fluxes; this feedback could be incorporated in our model by assuming a wind speed dependence in c_q. In addition, the Hadley circulation may be better viewed as a coupled problem (Satoh 1994; Held 2001) in which the SST is interactively determined by the surface energy balance of the ocean, and ultimately, the variation of insolation with latitude. In this case, the natural scale of the Hadley circulation could just be proportional to the radius of the earth.

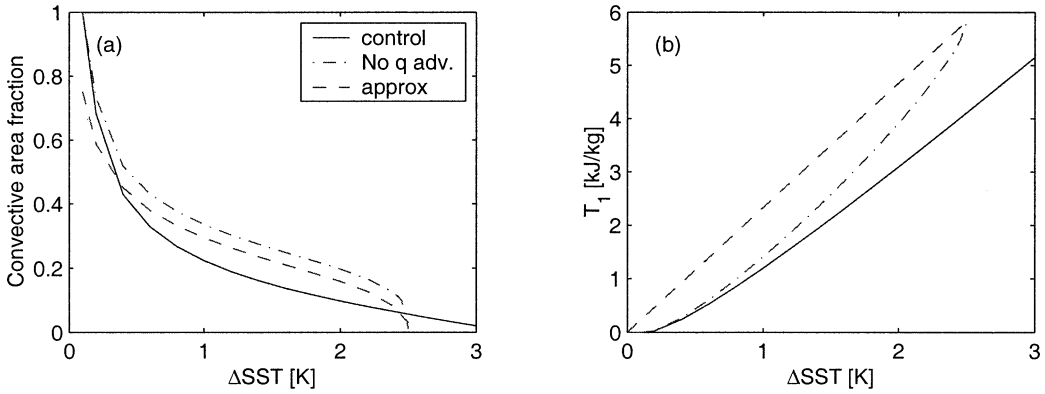

FIG. 6. Variation of the (a) convective area fraction and (b) scaled tropospheric temperature (in energy units) vs ΔSST. The solid curve shows the control model (including cloud radiative feedbacks), the dot–dash curve shows the control model without horizontal moisture advection, and the dashed line shows the closed-form approximations (39) and (40).

d. The convective area fraction

This study was in part motivated by a desire to understand what factors control the fraction of the Tropics that support significant deep convective precipitation on monthly and longer timescales. In our model, the convective area fraction is exclusively determined by ΔSST and the strength of cloud radiative feedback. The solid line in Fig. 6a shows how the convective area fraction depends on ΔSST, with cloud radiative feedback included. Surprisingly, the convective area decreases steadily to zero at a critical ΔSST slightly in excess of 3.2 K, and there is no physically meaningful solution for larger ΔSST. This peculiar behavior is a consequence of the decrease in effective gross moist stability M_{eff} and the corresponding increase in the convergence feedback in our model as T_1 increases. The tropospheric temperature T_1 (solid line in Fig. 6b) increases with ΔSST, driven by the localization of the convectively active region to higher SSTs. As ΔSST increases, $M_{\text{eff}}(T_1)$ decreases, and the convective region narrows and intensifies. When ΔSST reaches 3.2 K, T_1 reaches 5 kJ kg^{-1}, which is the threshold at which M_{eff} becomes negative (and radiative–convective instability of a horizontally uniform convecting state would become possible). At this point, the convergence feedback becomes infinite, narrowing the convective region into a single column. This threshold temperature (and hence the maximum allowable ΔSST) is very sensitive to the exact choices of gross moist stability and cloud–radiation feedback parameter. The prediction that M_{eff} becomes negative as the tropopause warms may well be an model artifact.

The domain-averaged latent heating must in all cases balance the radiative cooling. This implies that $\overline{P} = \overline{R} = R^{\text{clr}} - r\overline{P}$, so $\overline{P} = R^{\text{clr}}/(1 + r)$. Since R^{clr} is specified except for a slight increase with the tropospheric temperature, $\overline{P}$ is only weakly dependent on ΔSST, increasing 13% over the plotted range of ΔSST. Hence, a small convective area fraction goes along with high precipitation rates within the convective region.

The dot–dashed lines in Fig. 6 show the area fraction and tropospheric temperature when horizontal moisture advection is neglected. At any given ΔSST, the tropospheric temperature is slightly higher without moisture advection, and over most of the plotted range of ΔSST the fractional area of convection is substantially larger. However, both curves show a similar qualitative dependence on ΔSST as in the control case. The area fraction reaches zero at a somewhat smaller critical value of ΔSST = 2.5 K, because T_1 is slightly higher for a given ΔSST in this case.

Simple approximate formulas for the convective area fraction and tropospheric temperature, when horizontal moisture advection is neglected and the convective area fraction is small, are derived in the appendix:

$$T_1 = a_1 c_p \Delta\text{SST}, \tag{39}$$

$$\frac{A_c}{A} = \left\{ \frac{a_2 P_0}{c_p \Delta\text{SST}[1 + C(T_1)]} \right\}^{1/3}. \tag{40}$$

(The terms a_1 and a_2 are nondimensional combinations of thermodynamic parameters derived in the appendix and given in Table 1.) These are plotted in Fig. 6 as dashed lines. They reproduce the qualitative behavior of the exact solutions even when the convective area fraction is fairly large. We have already explained the rise of tropospheric temperature with ΔSST as due to its control by convection over the highest SSTs. The convective area fraction decreases as ΔSST or the convergence feedback increases; the latter effect dominates for ΔSST exceeding 1 K with our parameter choices, due to the sensitivity of convergence feedback to T_1. Since the convergence feedback is inversely proportional to the effective gross moist stability, this reemphasizes the importance of the latter for controlling the convective area fraction.

6. Discussion and conclusions

In this paper we have tried to demonstrate the utility of the WTG approximation for understanding an ide-

alized nonlinear Walker circulation with interactive deep convection and a simple empirically based cloud–radiation feedback, and determining over which parts of the domain deep convection will be active. The Walker circulation is forced by a specified sinusoidal spatial variation of SST. We have used a particularly simple ''hard moist convective adjustment'' parameterization in which the atmosphere is forced to have a fixed relative humidity profile in convective regions. We follow the dynamical framework of the QTCM, including only a single allowable vertical mode of humidity variability outside convective regions.

The WTG approximation is that the tropospheric temperature is essentially uniform (though unknown) across the domain. In each tropospheric column undergoing deep convection, the vertical motion can be diagnosed from the moist static energy budget as a function of the tropospheric temperature; in dry regions, the subsidence rate is similarly diagnosed from the radiative-subsidence energy balance. The moisture profile is tied to the tropospheric temperature in the convective regions, and is a balance of advection and surface evaporation outside. Global mass and moisture balance allow one to deduce the tropospheric temperature, convective area fraction, and the divergent flow using a relatively simple numerical algorithm. The WTG approximation is tested a posteriori by calculating the tropospheric temperature perturbations consistent with the pressure gradients required to drive the flow diagnosed by WTG.

Unless SST variations are extremely weak, convection is totally suppressed over the coldest parts of the domain. Inclusion of cloud–radiation feedback localizes the convection into a much smaller area over the warmest water, and raises the tropospheric temperature correspondingly. The convective area fraction with and without cloud–radiation feedback compares quite well with G00's similarly forced CRM simulation. As the SST difference between warm and cold pools increases, the convective area fraction decreases. For a sufficiently large SST differential, the model no longer admits a physically meaningful solution, though this conclusion may be a model artifact related to simplistic assumptions about the dependence of gross moist stability on tropospheric temperature.

The solutions are quite sensitive to the cloud–radiation feedback parameter. While the cloud–radiation feedback formulation used here is inspired by existing observations, the observations do not perfectly constrain this feedback parameter. The gross moist stability also varies significantly within the convectively active parts of the Tropics. Plausible choices of the radiative feedback parameter and the gross moist stability admit the possibility of ''effective gross moist instability,'' in which the net effect of upward motion is to increase column-mean moist static energy. This creates a runaway feedback that prevents a steady-state solution to the model discussed in this paper. Observational studies of the moist static energy balance of those regions of the Tropics with the lowest gross moist stability (e.g., Tian et al. 2001) should provide more insight into the physical relevance of this mechanism. Strong radiative–convective feedback or instability could even provide the basis for an coupled ocean–atmosphere oscillator, in which the radiative feedback leads to persistent deep convection over a warm part of the oceans, reducing surface insolation and cooling the oceans until convection can no longer be supported. After a suppressed period, the ocean might then heat up enough to allow the cycle to be repeated. Conceivably, such a mechanism could be helping to excite intraseasonal variability over the Indian and west Pacific Oceans, although the oceanic heat budget over these regions is responding to many other factors as well (Fasullo and Webster 1999).

The WTG approximation is quite accurate for the domain size used here (2000 km) and no ambient rotation. For a domain size of 20 000 km (the extreme case of a tropical Walker circulation between a cold SST Western Hemisphere and a warm SST Eastern Hemisphere), the horizontal temperature gradients required to drive a purely baroclinic flow against surface drag would become comparable to the SST variations in our idealized model. However, in reality most of the drag is confined to the lowest 1500 m of the atmosphere, reducing the required pressure gradients in the free troposphere such that WTG remains a useful approximation (Sobel and Bretherton 2000).

The observed Walker circulation is a tightly coupled ocean–atmosphere phenomenon. We are examining a version of our model coupled to an oceanic mixed layer whose heat budget includes a simple representation of the surface radiation effects of deep convective cloud systems, with SST variations forced by a specified x-varying oceanic heat export. Ocean coupling can remove some unrealistic features of our atmosphere-only simulation. In particular, reduced shortwave heating under intense convection prevents the convection from focusing to zero fractional area, as can happen in our atmosphere-only model.

Other extensions to the model could be pursued, including a frictional boundary layer, radiative feedbacks of boundary layer clouds over colder SSTs, the effect of mean wind speed on bulk transfer coefficients, and the observed correlation of mean moisture profile with mean precipitation in convective regions (Fuchs and Raymond 2002). Much of the model behavior could be distilled into a two-box approximation analogous to that of Kelly and Randall (2001), providing a simpler context for these extensions. Another possible extension is to the Hadley circulation case of a north–south-oriented domain, including weak ambient rotation, following in the path of Held and Hou (1980), Satoh (1994), and Fang and Tung (1996), with more emphasis on thermodynamic consistency between the large-scale circulation and deep convection.

Acknowledgments. We acknowledge useful discussions with Isaac Held (who helped us clarify the fundamental role of moisture advection in this problem), Steve Krueger (who provided the COARE radiation dataset). Matthew Peters, David Neelin, and insightful reviews by David Raymond and Kerry Emanuel. We were supported by NASA Grant NAGS5-10624, NSF Grant ATM-0096195, and a Packard Foundation Fellowship for Science and Engineering granted to AHS.

APPENDIX

Approximate Formulas for Convective Area Fraction and Tropospheric Temperature

If we neglect moisture advection, the precipitation decreases smoothly to zero at the edge of the convective region. Within the convective region, the precipitation is given by (29) in terms of the unknown T_1. We can use this equation to solve for both the convective edge and the area-integrated precipitation within the convective region. We must then choose the T_1 for which the solution satisfies domain-averaged heat balance, $\overline{P} = R^{\mathrm{clr}}/(1 + r)$. Let $f_c = A_c/A$ be the unknown convective area fraction, or equivalently the nondimensionalized location of the convective edge. Substituting $P = 0$ in (29), the convective edge location is where

$$0 = P_0 + [c_q \gamma_s c_p \Delta\mathrm{SST} \cos(\pi f_c) - \alpha T_1)(1 + C(T_1)], \tag{A1}$$

where

$$\alpha = c_q b_s + c_R/(1 + r). \tag{A2}$$

Using (29) to find $\overline{P}$, the heat balance constraint is

$$\begin{aligned}\frac{R^{\mathrm{clr}}}{(1 + r)} &= \overline{P} \\ &= \int_0^{f_c} \{P_0 + [c_q \gamma_s c_p \Delta\mathrm{SST} \cos(\pi\xi) - \alpha T_1] \\ &\qquad \times (1 + C)\}\, d\xi \\ &= \int_0^{f_c} c_q \gamma_s c_p \Delta\mathrm{SST}[\cos(\pi\xi) - \cos(\pi f_c)] \\ &\qquad \times (1 + C)\, d\xi \\ &= c_q \gamma_s c_p \Delta\mathrm{SST}(1 + C)F(f_c),\end{aligned}$$

$$F(f_c) = \sin(\pi f_c)/\pi - f_c \cos(\pi f_c). \tag{A3}$$

The left-hand side can be simplified by noting

$$\begin{aligned}R^{\mathrm{clr}}/(1 + r) &= R_0^{\mathrm{clr}}/(1 + r) + c_R T_1/(1 + r) \\ &= P_0 + c_R T_1/(1 + r).\end{aligned}$$

We now approximately solve (A1) and (A3), assuming the convective area fraction is small. In this case, $F(f_c)$ can be approximated by the leading term in its Taylor series:

$$F(f_c) \approx \pi^2 f_c^3/3, \text{ for } f_c \ll 1. \tag{A4}$$

This is in fact a reasonable approximation even for f_c as large as 0.5. In addition, we can take $\cos(\pi f_c) \approx 1$ in (A1) to obtain a relation between ΔSST and T_1:

$$c_q \gamma_s c_p \Delta\mathrm{SST} \approx \alpha T_1 - P_0/[1 + C(T_1)].$$

If the convective area fraction is to be small, the precipitation in the convective region must be large; this requires that the convergence feedback be large, so the second term on the right-hand side be small. Making this approximation, we obtain the first desired approximate relationship,

$$c_q \gamma_s c_p \Delta\mathrm{SST} \approx \alpha T_1,$$

which is equivalent to (39) with

$$a_1 = c_q \gamma_s/\alpha. \tag{A5}$$

The approximation for the area fraction is obtained by substituting the Taylor expansion (A4) into the heat balance equation (A3), neglecting the small temperature dependence of R^{clr} that shows up on the left-hand side:

$$P_0 \approx c_q \gamma_s c_p \Delta\mathrm{SST}(1 + C)\pi^2 f_c^3/3.$$

The desired approximate formula (40) is obtained by solving this equation for f_c; the constant a_2 in that formula is seen to be

$$a_2 = 3/(\pi^2 c_q \gamma_s). \tag{A6}$$

REFERENCES

Burks, J., 1998: Radiative fluxes and heating rates during TOGA COARE over the intensive flux array. M.S. thesis, Dept. of Meteorology, University of Utah, 85 pp.

Carr, M. T., and C. S. Bretherton, 2001: Convective momentum transport over the tropical Pacific: Budget estimates. *J. Atmos. Sci.,* **58,** 1673–1693.

Clement, A., and R. Seager, 1999: Climate and the tropical oceans. *J. Climate,* **12,** 3383–3401.

Emanuel, K. A., 1987: An air–sea interaction model of intraseasonal oscillations in the tropics. *J. Atmos. Sci.,* **44,** 2324–2340.

——, J. D. Neelin, and C. S. Bretherton, 1994: On large-scale circulations in convecting atmospheres. *Quart. J. Roy. Meteor. Soc.,* **120,** 1111–1143.

Fang, M., and K. K. Tung, 1996: A simple model of nonlinear Hadley circulation with an ITCZ: Analytic and numerical solutions. *J. Atmos. Sci.,* **53,** 1241–1261.

Fasullo, J., and P. J. Webster, 1999: Warm pool SST variability in relation to the surface energy balance. *J. Climate,* **12,** 1292–1305.

Fuchs, Z., and D. J. Raymond, 2002: Large-scale modes of a nonrotating atmosphere with water vapor and cloud–radiation feedbacks. *J. Atmos. Sci.,* **59,** 1669–1679.

Grabowski, W. W., J.-I. Yano, and M. W. Moncrieff, 2000: Cloud-resolving modeling of tropical circulations driven by large-scale SST gradients. *J. Atmos. Sci.,* **57,** 2022–2039.

Held, I. M., 2001: The partitioning of the poleward energy flux between the tropical ocean and atmosphere. *J. Atmos. Sci.,* **58,** 943–948.

——, and A. Y. Hou, 1980: Nonlinear axially symmetric circulations in an almost inviscid atmosphere. *J. Atmos. Sci.,* **37,** 515–533.

Kelly, M. A., and D. A. Randall, 2001: A two-box model of a zonal

atmospheric circulation in the Tropics. *J. Climate,* **14,** 3944–3964.

Kiehl, J. T., 1994: On the observed near cancellation between longwave and shortwave cloud forcing in tropical regions. *J. Climate,* **7,** 559–565.

Larson, K., D. L. Hartmann, and S. A. Klein, 1999: The role of clouds, water vapor, circulation, and boundary layer structure in the sensitivity of the tropical climate. *J. Climate,* **12,** 2359–2374.

Lin, X., and R. H. Johnson, 1996: Heating, moistening, and rainfall over the western Pacific warm pool during TOGA COARE. *J. Atmos. Sci.,* **53,** 3367–3383.

Lindzen, R. S., and S. Nigam, 1987: On the role of sea surface temperature gradients in forcing low-level winds and convergence in the tropics. *J. Atmos. Sci.,* **44,** 2418–2436.

Miller, M. J., A. C. M. Beljaars, and T. N. Palmer, 1992: The sensitivity of the ECMWF model to the parameterization of evaporation from the tropical oceans. *J. Climate,* **5,** 418–434.

Miller, R. L., 1997: Tropical thermostats and low cloud cover. *J. Climate,* **10,** 409–440.

Neelin, J. D., and N. Zeng, 2000: A quasi-equilibrium tropical circulation model—Formulation. *J. Atmos. Sci.,* **57,** 1741–1766.

——, I. M. Held, and K. H. Cook, 1987: Evaporation–wind feedback and low-frequency variability in the tropical atmosphere. *J. Atmos. Sci.,* **44,** 2341–2348.

Pierrehumbert, R. T., 1995: Thermostats, radiator fins, and the local runaway greenhouse. *J. Atmos. Sci.,* **52,** 1784–1806.

Polvani, L. M., and A. H. Sobel, 2002: The Hadley circulation and the weak temperature gradient approximation. *J. Atmos. Sci.,* **59,** 1744–1752.

Raymond, D. J., 2000: The Hadley circulation as a radiative–convective instability. *J. Atmos. Sci.,* **57,** 1286–1297.

Satoh, M., 1994: Hadley circulations in radiative–convective equilibrium in an axially symmetric atmosphere. *J. Atmos. Sci.,* **51,** 1947–1968.

Sobel, A. H., and C. S. Bretherton, 2000: Modeling tropical precipitation in a single column. *J. Climate,* **13,** 4378–4392.

——, J. Nilsson, and L. M. Polvani, 2001: The weak temperature gradient approximation and balanced tropical moisture waves. *J. Atmos. Sci.,* **58,** 3650–3665.

——, I. Held, and C. S. Bretherton, 2002: The ENSO signal in tropical tropospheric temperature. *J. Atmos. Sci.,* **59,** 2702–2706.

Su, H., and J. D. Neelin, 2002: Teleconnection mechanisms for tropical Pacific descent anomalies during El Niño. *J. Atmos. Sci.,* **59,** 2682–2700.

Tian, B., G. J. Zhang, and V. Ramanathan, 2001: Heat balance in the Pacific warm pool atmosphere during TOGA COARE and CEPEX. *J. Climate,* **14,** 1881–1893.

Wang, B., and T. Li, 1993: A simple tropical atmosphere model of relevance to short-term climate variations. *J. Atmos. Sci.,* **50,** 260–284.

Xie, P., and P. A. Arkin, 1997: Global precipitation: A 17-year monthly analysis based on gauge observations, satellite estimates, and numerical model outputs. *Bull. Amer. Meteor. Soc.,* **78,** 2539–2558.

Zebiak, S. E., 1986: Atmospheric convergence feedback in a simple model for El Niño. *Mon. Wea. Rev.,* **114,** 1263–1272.

Zeng, N., J. D. Neelin, and C. Chou, 2000: Quasi-equilibrium tropical circulation model—Implementation and simulation. *J. Atmos. Sci.,* **57,** 1767–1796.